

Optimum design of miniature platforms for marginal fields

Sha Miao, Yuming Liu* and Dick K.P. Yue

Department of Mechanical Engineering, Massachusetts Institute of Technology, Cambridge, MA 02139, USA

(Received May 3, 2021 Revised May 24, 2021, Accepted June 6, 2021)

Abstract. Motivated by many recent discoveries of marginal fields in deep water, this paper presents a novel and economical design concept of a minimal floating platform with around 10,000 cubic tons in displacement. The concept characterizes a simple hull geometry and an excellent seakeeping behavior. It incorporates a damping plate at the keel on the basis of a spar-like floater. The design procedure is explained and illustrated. The paper also describes a new design methodology that is capable of efficiently evaluating the seakeeping performance of the platforms with the viscous damping effect included. We integrate this methodology into an Evolutionary Algorithm (EA) to conduct a multi-objective optimization for our novel design. The hull shape is optimized by minimizing the heave motion in waves without sacrificing the cost in construction and installation. Several potential geometric configurations are considered. The optimization results provide a wealth of information that can be used to support practical design decisions.

Keywords: mini-platforms; marginal fields; damping plate; multi-objective optimization

1. Introduction

Global demand for hydrocarbons is expected to increase by 5% per year for the next decades (Cermelli *et al.* 2004). However, the likelihood of discovering large oil and gas fields is decreasing. On the other hand, the inventory of undeveloped small fields keeps growing recently, especially in deep water. The deferral of these discoveries is mainly due to the fact that the construction expenses of platforms and pipeline infrastructure are usually beyond the value of the oil or gas the reserves contain. Such reserves are referred as “marginal fields”.

Semi-submersible platforms, tension leg platforms (TLP) and spars are the main surface support platforms for deep water developments at present. Semi-submersible platforms achieve the stability by large displacements, thereby associated with high construction cost. In addition, the large displacement requires expensive mooring systems, which increase significantly in size and cost with water depth. TLPs limit the heave and pitch motions by a set of vertical steel tendons. Numerous mini-TLP concepts have been invented for the marginal oil fields, such as Seastar mini-TLP and Modec mini-TLP. However, this design cannot be easily extended to ultra-deep water greater than $\sim 5,000$ ft due to the high costs for the tendon installation. Spars usually minimize the heave motion by a deep draft of around 100 \sim 200 meters. The cost for installation and fabrication of spars is

*Corresponding author, Senior Research Scientist, E-mail: yuming@mit.edu

generally high because of the large size of the hull, and the difficulties of upending the platform and integrating the topsides offshore.

To circumvent the high cost of the existing platforms, one prime objective of the present research is to identify an economical design concept that has a satisfactory seakeeping characteristic in deep water. We propose a novel design of a minimal floating offshore platform with a displacement around 10,000 metric tons. This new concept combines a small and simple spar-like floater with a heave plate at the keel. The small size and the simple geometric shape reduce the cost of construction and installation significantly. The damping plate at the keel further improves the platform response by increasing the added mass and introducing viscous damping.

Linear wave theory in the frequency domain generally provides a satisfactory and efficient prediction for the wave-induced loads on the offshore platforms in the mild sea condition. Panel codes like WAMIT (King 1987, Newman and Sclavounos 1988, Newman 1992) are hence widely used to explore the design space and to obtain fundamental insights of the hydro-dynamics at the initial design phase of the offshore systems. However, viscous damping effect is not directly considered in WAMIT. Since the damping due to the heave plate is utilized to suppress the heave motion in our novel design, an effective and accurate viscous model is needed to account for this effect. Classical offshore hydrodynamic analysis usually considers this effect by invoking simple empirical formulas with unknown coefficients to be determined either with scaled model tests or direct Navier-Stokes-based numerical simulation that requires excessive computational time. This paper develops an accurate and effective model, “Discrete Vortex Ring Model (DVRM)”, to efficiently evaluate the viscous damping due to the heaving plate. This model is an extension of the two-dimensional “single vortex model” (Brown and Michael 1955, Faltinsen and Sortland 1987, Stiassnie *et al.* 1984) to the axisymmetric oscillation problem. A new design methodology is then developed based on the combination of WAMIT and DVRM to analyze the hydrodynamics of the miniature platforms. The reduced computational costs of the proposed methodology in evaluating the viscous damping effect allow us to perform large numbers of analysis on platforms with different spar and heave plate geometries/configurations.

We first prove the feasibility of our design concept. We enumerate a number of geometry modifications and evaluate the hydrodynamic performance using the proposed methodology. An acceptable design is then compared with a short- draft spar with the same displacement to show the advantages of our design. Though feasible, the design we obtain may still be far from the optimal solution. Several applications in optimizing seakeeping behavior have been reported (Chou 1977, Akagi and Ito 1984, Kagemoto 1992, Clauss and Birk 1996). Most of the work is restricted to single-objective optimization. The goal of the present research is to minimize both the heave motion amplitude and the costs for the mini-platform from geometric design consideration. This is a multi-objective optimization problem in which the two objectives are in general conflicting. Evolutionary algorithm (EA) is a suitable approach to deal with this kind of optimization problems. Birk (2009) successfully applies the ε – MOEA (Deb *et al.* 2003) to the multi-objective hydrodynamic optimization of the offshore structures. The viscous damping effect, however, is generally neglected. Our work integrates the proposed design methodology into this EA optimization algorithm to find the optimum design based on our new design concept with the viscous damping effect accounted for. This paper also applies this optimization to the investigation of other similar potential geometries. Optimal designs based on different configurations for the mini-platforms are obtained and discussed.

2. Conceptual design for the mini-platform

We aim at designing a miniature floating platform for deep water operation, which has a displacement of around 10, 000 metric tons, a simple hull geometry, and a satisfactory motion performance. The basic idea of our design is to combine the features of a small spar-type platform with a damping plate at the keel. Classical spar platforms with constant cross section achieve their ideal small motion responses in waves with the use of deep draft and/or large displacement. Direct extension of this design for mini-platforms leads to non-economical structures for marginal fields. We thus search for alternative designs for mini-platforms with simple hull shape similar to the traditional spars.

2.1 Preliminary design considerations

Limited by the small displacement, we define our mini-platform for production only with a rate of 30k Barrels per Day (bpd). A sketch of the preliminary configuration of the mini-platform is shown in Fig. 1. The platform is composed of three parts: a multi-level deck above the waterline, a hull with a moonpool inside, and a heave plate attached at the keel of the hull.

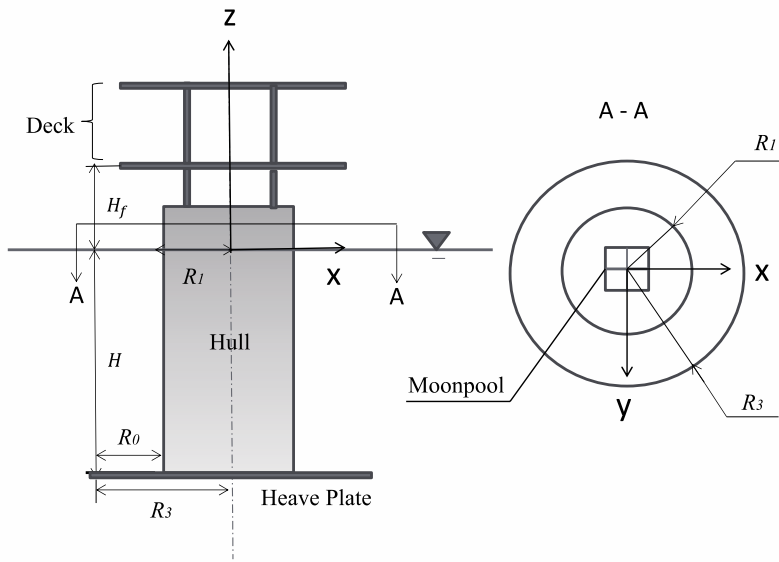


Fig. 1 General configuration and definition of the dimensions of a miniature floating platform

Table 1 Estimates of the main dimensions for the mini-platform

| Cross section | Draft | Freeboard | Deck |
|---------------|--------------|---------------|--------------------------------|
| $R_1 \geq 7m$ | $H \sim 30m$ | $H_f \sim 9m$ | $27.4m \times 27.4m \times 6m$ |

Table 2 Estimates of the weight distribution for the mini-platform

| Displacement | Topside | Hull |
|---------------------------|-----------------------|-----------------------|
| $\nabla \sim 10,000$ tons | $W_T \sim 2,500$ tons | $W_H \sim 2,800$ tons |

Several miniature platforms have been constructed to date, most of which belong to mini-TLPs. Based on these statistics (Hudson *et al.* 1996, Wilhoit and Supan 2010, Kibbee *et al.* 1999, Kibbee *et al.* 2010, Koon *et al.* 2002, Ronalds *et al.* 2010) and the design codes (API-RP2A-WSD 2006, API-RP2A-WSD 2000, ABS-MODU 2012), we obtain an estimate of the main dimensions and weight distribution, which are listed in Tables 1 and 2. The details on the estimate of these quantities can be found in Miao (2013).

Once the initial dimensions and weights are established, the hydrostatic stability and hydrodynamic analysis can be performed. The metacentric height is examined to meet the stability criteria during all phases of design.

2.2 Development of the hull shape

The suppression of heave motion of a floating platform can be achieved by (1) increasing the heave natural period away from the peak wave frequency; (2) reducing the wave exciting force; and (3) increasing the damping of the system.

- (1) Increasing the heave natural period of a platform can be achieved by shrinking the water-plane area and increasing the added mass. The added mass of a cylindrical buoy is mainly due to the end effect, which can be approximated as the displaced fluid mass of a half sphere of the diameter of the keel. This motivates us to change the classical spar into a design with non-constant cross sections. To avoid complicating the construction, we first consider a hull composed of two cylinders with radius R_1 and R_2 , respectively ($R_2 > R_1$). A thin damping plate can be attached at the keel to further increase the added mass without increasing the displacement significantly (see Fig. 2(a)).
- (2) The wave exciting force may be reduced by applying a shoulder into our design. The dynamic pressure force acting on this shoulder to some extent can counteract the exciting force at the keel (see Fig. 2 (b)) (Haslum *et al.* 1999). Due to the exponential decay in dynamic pressure with water depth, a shoulder close to the water surface is more effective. However, such a horizontal shoulder introduces a rapid variation in the cross section. It should be submerged deep enough to be prevented from penetrating the free surface. The metacentric height is another limiting factor for the position of the shoulder. With these two concerns, we may modify the shoulder from horizontally to obliquely displaced (see Fig. 2(c)).

- (3) To mitigate the heave motion, we utilize the viscous damping effect in our design by attaching a thin heave plate at the keel. This results in flow separation at the sharp edge of the plate and the associated damping effect is estimated by a newly-developed model “Discrete Vortex Ring Model (DVRM)” which will be presented in the next section.

Based on all the above three considerations, we obtain a configuration for the mini-platform shown as design (d) in Fig. 2. We remark that in the hydrodynamic analysis presented in this paper, the bottom of the moonpool is assumed to be closed by the riser-guide plate (as in operation) so that the water inside the moonpool is treated as trapped mass to oscillate together with the platform in waves. In the estimate of the vertical center of gravity (VCG) of the platform, we assume that (i) the center of mass of the topside is located at 2.0 m above the bottom deck, (ii) the center of mass of the ballast and mooring is at the keel of the platform, and (iii) the masses of the hull and damping plate are uniformly distributed on the hull surface and damping plate. The weight of the ballast and mooring together with the weight of the platform is balanced by the displacement of the hull (excluding the water trapped in the moonpool). With these weight distributions in the vertical direction, we can easily determine the VCG of the platform and the radius of gyration for pitch (and roll) motion of the platform. The vertical center of buoyancy (VCB) of the platform is simply the geometric center of the submersible volume of the platform. Once VCG, VCB and waterplane area are known, the metacentric height (GM) are readily determined.

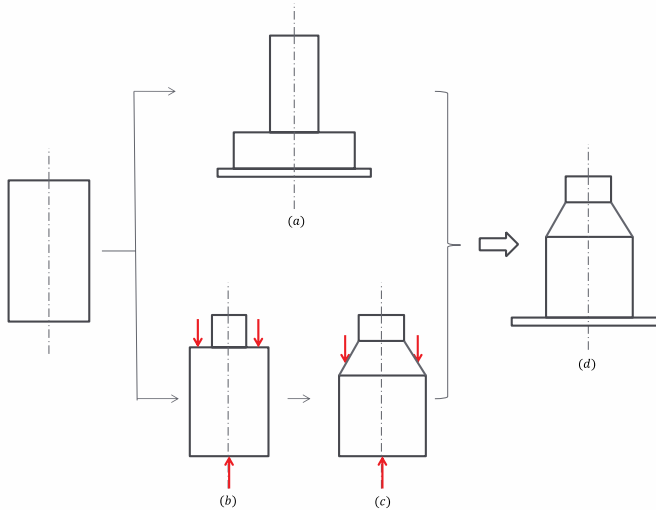


Fig. 2 Summary of the hull evolution from a classical spar to the final configuration of the mini-platform

3. Hydrodynamic models and numerical methods

This section describes a new design method for predicting the linear frequency response of the platform with viscous effects included based on the combination of WAMIT and DVRM.

Under operational conditions where the amplitudes of incident waves and body motions are relatively small, linear wave theory in the frequency domain is valid and useful in capturing the hydrodynamic effects in wave-body inter-actions. At the initial stage of the design, we ignore the effects due to risers, moorings and the moonpool. Then the heave motion equation of the platform in regular waves, which is the most significant concern for spar-type floaters, can be expressed in the form

$$(M + A_{33})\ddot{\xi}_3 + B_{33}^P \dot{\xi}_3 + B_{33}^V |\dot{\xi}_3 - v_f|(\dot{\xi}_3 - v_f) + C_{33}\xi_3 = X_3 \quad (1)$$

where M is the mass of the platform, ξ_3 is the displacement of the platform due to heave motion; v_f is the vertical component of the fluid velocity of the ambient flow (including the wave diffraction effect) at the edge of the damping plate; A_{33} is the added mass coefficient; B_{33}^P is the linear wave damping coefficient; B_{33}^V is the viscous damping coefficient related to the flow separation at the edge of the damping plate; and X_3 is the heave wave exciting force.

To compute the force coefficients in (1), we decompose this problem into two sub-problems. One is the well-known wave radiation/diffraction problem which is associated with all the linear hydrodynamic coefficients. Potential flow models can be efficaciously employed to solve this sub-problem. The other is the viscous damping problem with the nonlinear term $B_{33}^V |\dot{\xi}_3 - v_f|(\dot{\xi}_3 - v_f)$ introduced by the damping plate. A new model, DVRM, which efficiently estimates B_{33}^V , is described in details below.

3.1 Potential flow model

For the first sub-problem, due to the linearity and harmonic time dependence of this problem, the total velocity potential can be decomposed into radiation and diffraction components (Newman 1977, Lee 1995). By using Green's theorem we can derive the integral equations for these two components on the body boundary. Panel method is usually applied to solve these equations (Lee 1995, Newman and Lee 2002). The linear hydrodynamic coefficients in Eq. (1) are subsequently computed. We here use the standard radiation/diffraction code WAMIT to solve for all the hydrodynamic coefficients.

3.2 Vortex damping model

As for the second sub-problem, for simplicity, we ignore the interference effect of the hull on the damping plate and only consider an infinitely thin plate with radius R oscillating with velocity $V = V_0 \sin(2\pi t/T)$ in an unbounded, inviscid and otherwise undisturbed fluid, where V_0 is the velocity amplitude of plate oscillation and T is the period. The two dimensionless parameters governing this three-dimensional axisymmetric problem are the Keulegan-Carpenter number $KC = V_0 T / R$ and the total force coefficient $C_{Fv} = F / (0.5 \rho V^2 \pi R^2)$, where F is the total hydrodynamic force exerted on the plate and ρ is the fluid density. Here we confine our interest to the separated flow at KC up to ~ 10 .

The following vortex pattern is observed in experiments for a fixed thin disk in oscillatory flow at low KC number (Lake *et al.* 2000, Bernardinis *et al.* 1981). During the first half cycle, the vorticity shed tends to roll up into a single vortex ring. As the flow slows down, the flow at the edge of the disk reverses and a second vortex sheet of opposite magnitude starts to emanate, and be shed at the second half cycle. At the same time, the first vortex ring is interacting with the second ring to form a vortex ring pair, convecting away from the disk. The ring pair decays fairly fast due to the instability and viscous diffusion. The decay time scale t_d is of order of a period $O(T)$. It is a monotonically decreasing function of KC number and does not vary significantly with the Reynolds number R_e (Canals and Pawlak 2011). This whole pattern is repeated from cycle to cycle.

Motivated by the above observation, we develop a new highly efficient model, “DVRM,” to estimate the drag coefficient due to the flow separation occurring along the edge of the plate. We represent each vortex ring structure in the wake by a single vortex ring with a time-varying strength $\Gamma(t)$ plus a surface cut transporting the vorticity to this vortex ring. This is a three-dimensional extension of the single vortex model that is first proposed by Brown & Michael (Brown and Michael 1955). A bound vortex ring sheet is distributed with unknown strength $\gamma(r, z, t)$ on the plate P . All the singularities should satisfy the following kinematic boundary condition

$$\int_P \gamma(r', z', t) [\tilde{v}_r n_r + \tilde{v}_z n_z] ds + \sum_i \Gamma_i [\tilde{v}_r n_r + \tilde{v}_z n_z] ds' = \mathbf{V} \cdot \mathbf{n} \quad (2)$$

where $\mathbf{n} = (n_r, n_z)$ is the unit normal vector of the plate P , and $(\tilde{v}_r, \tilde{v}_z)$ is the velocity at (r, z) induced by a unit vortex ring at (r', z') ([31]).

For each $\Gamma(t)$, the growth rate $d\Gamma/dt$ is determined by the unsteady Kutta condition (Nitsche and Krasny 1994) until $d\Gamma/dt$ changes sign

$$\frac{d\Gamma}{dt} = \frac{1}{2} (V_t^{-2} - V_t^{+2}) \quad (3)$$

where V_t^- and V_t^+ are the one-sided velocities at the separation point satisfying

$$V_t^- + V_t^+ = \bar{V}_t, \quad \frac{1}{2} (V_t^- - V_t^+) = \gamma(\mathbf{x}_e) \quad (4)$$

where \bar{V}_t is the averaged velocity, and $\gamma(\mathbf{x}_e)$ is the vortex sheet strength at the edge.

Meanwhile, the location of the growing vortex ring is determined by imposing the condition of zero total force on the ring plus the cut (Brown and Michael 1955)

$$\frac{dx_\Gamma}{dt} = \frac{1}{\Gamma} \left\{ \frac{d(\Gamma x_\Gamma)}{dt} - \mathbf{x}_e \frac{d\Gamma}{dt} \right\} \quad (5)$$

where \mathbf{x}_Γ is the location of $\Gamma(t)$.

After $d\Gamma/dt$ changes sign, the magnitude of the vortex ring starts to decay based on a decay model we proposed, while another structure of a vortex ring plus a cut starts to grow until $d\Gamma/dt$ for this vortex changes sign again. The decaying vortex ring convects with the local fluid velocity. The decay model is

$$\Gamma(t) = \Gamma_0 \exp \left\{ -KC \frac{t-t_0}{T} \right\} \quad (6)$$

where Γ_0 is the strength when $d\Gamma/dt$ changes sign at time t_0 .

DVRM has been validated extensively, and details can be found in (Miao 2013). By use of the DVRM simulation, we can obtain the steady-state solution of the force coefficient $C_{Fv}(t)$ as a function of KC efficiently. Fig. 3 shows a sample comparison of $C_{Fv}(t)$ due to vortex shedding of an infinitely thin circular disk oscillating in an unbounded, inviscid, and otherwise undisturbed fluid between the DVRM prediction and the existing result in De Bernardinis *et al.* (1981). They used a similar vortex ring sheet model, but applied a two-dimensional Kutta condition by assuming the vortex shedding to be governed by the flow characteristics near the geometrical singularity in the boundary. The present result agrees with the existing solution reasonably well. Based on the phase difference of added mass and damping effects, we can extract the drag force component from $C_{Fv}(t)$ (for a given KC), which then gives the damping coefficient B_{33}^V in Eq. (1) (Cozijn *et al.* 2005)

3.3 Heave motion response in ocean environments

With the combined use of WAMIT and DVRM, we can compute all the hydrodynamic coefficients in Eq. (1). Since the viscous damping effect is much more important than the wave damping for the proposed design, we ignore the B_{33}^P term. The damping effect on the motion response of the body is of critical importance only in the neighborhood of the natural frequency at which the inertial force cancels the restoring force. The body motion at the natural frequency (ω_n) is expected to be much larger than the ambient fluid motion. For simplicity, we approximate the relative velocity $\dot{\xi}_3 - v_f$ in Eq. (1) by the body velocity $\dot{\xi}_3$.

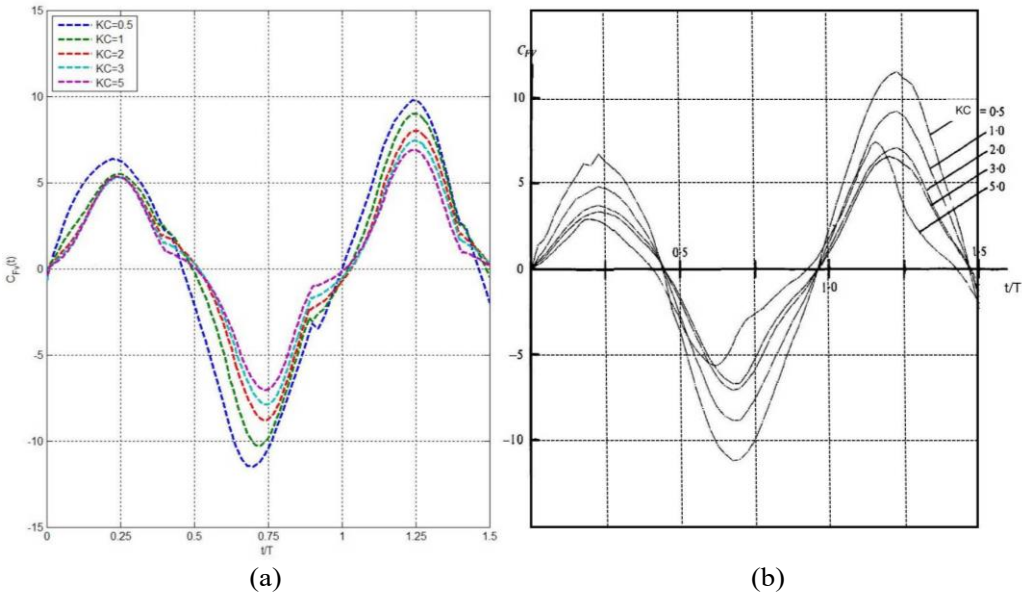


Fig. 3 Comparison of the time variation of the force coefficient C_{Fv} due to vortex shedding of an oscillating thin circular disk obtained: (a) by the present DVRM and (b) from De Bernardinis *et al.* (1981) for $KC = 0.5, 1, 2, 3$ and 5

Based on the concept of equivalent damping, we transfer the nonlinear viscous damping term associated with B_{33}^V into an equivalent linear damping term so that Eq. (1) can be solved in the frequency domain. We point out that the resulting equation for the unknown heave motion amplitude is still quadratic (for a given value of B_{33}^V) since the equivalent damping is applied at any body motion amplitude.

The resulting quadratic equation can be solved analytically (Sadeghi *et al.* 2004). For given B_{33}^V , the response amplitude operator (RAO) of the heave motion is obtained as

$$RAO = \frac{1}{\bar{A}} \left\{ \frac{-b + \sqrt{b^2 + 4ac}}{2a} \right\}^{\frac{1}{2}} \quad (7)$$

where \bar{A} represents the amplitude of regular incoming wave (at frequency ω), and

$$a = \left(\frac{8}{3\pi} \omega^2 B_{33}^V \right)^2, \quad b = [C_{33} - \omega^2(M + A_{33})]^2, \quad c = |X_3|^2 \quad (8)$$

The solution of RAO in (7) has a nonlinear dependence on \bar{A} since the coefficient c has a quadratic dependence on \bar{A} . Since the damping coefficient B_{33}^V is a function of KC that varies linearly with the heave motion amplitude, RAO for given \bar{A} and ω is determined through a simple iteration with the use of (7). Note that the relative velocity of the body (to the fluid particle) in the evaluation of viscous damping can actually be considered in the iterative procedure. In this case, Eq. (1) needs to be solved numerically while RAO in (7) cannot be directly used.

In irregular seas, a rigorous procedure to account for the quadratic viscous damping is the use of so-called stochastic linearization together with iteration on the standard deviation of the heave relative velocity as in regular waves. Since the viscous damping plays a critical role only in the narrow neighborhood of the natural frequency, we propose a simplified approximate procedure to evaluate the significant heave response in irregular seas, which allows us to study the optimal design of mini-platforms. As an example, we use the Modified Pierson-Moskowitz spectrum (Michel 1999) to describe the ocean environment for design. We divide the incident wave spectrum into two parts: $S(\omega) = S_1(\omega) + S_2(\omega)$ where $S_1(\omega) = S(\omega)$ for $\omega \in [\omega_n - \Delta\omega/2, \omega_n + \Delta\omega/2]$ while $S_1(\omega) = 0$ outside this frequency range, and $S_2(\omega) = S(\omega) - S_1(\omega)$. The energy of $S_1(\omega)$ is then approximated by a single wave component at frequency ω_n . The motion height resulted from this wave component (ξ_{s1}) is obtained by the iterative procedure in regular waves (described above). The motion resulted from $S_2(\omega)$ is obtained simply by the linear theory as the viscous damping effect can be neglected away from ω_n . The total significant height of the heave motion ξ_s is

$$\xi_s = \xi_{s1} + 4 \left[\int_0^\infty S_2(\omega) |RAO(\omega)|^2 d\omega \right]^{\frac{1}{2}}. \quad (9)$$

In the following, ξ_s is used as a metric to measure the motion performance of the platform. In this study, based on the RAO results shown in Fig. 5, we choose $\Delta\omega = 2\pi/(T_n - 1) - 2\pi/(T_n + 1)$ corresponding to a range of two seconds around the natural period $T_n = 2\pi/\omega_n$.

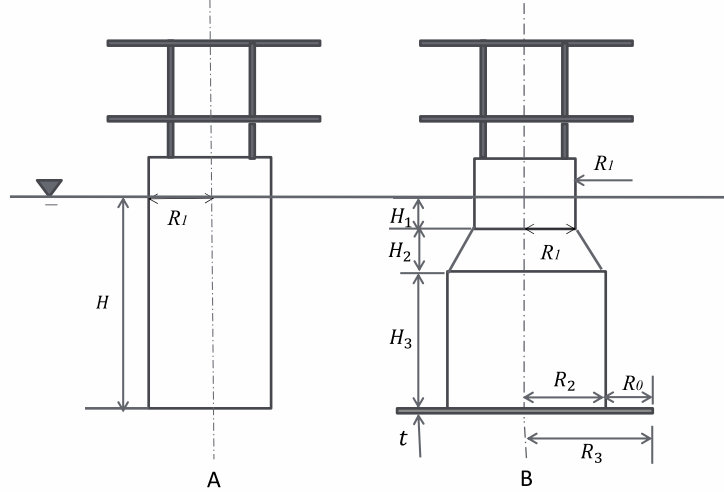


Fig. 4 Sketch of the miniature platform B and the short-draft spar A with identical displacement $\Delta = 12,000$ metric tons and draft $H = 30\text{ m}$

4. Feasibility of the concept of the mini-platform

We obtain several reasonable designs by trial and error with the proposed design methodology. We here compare the heave motion performance of one sample design of the mini-platforms with a short-draft (classical) spar to show the feasibility of our design concept. The mini-platform and the short-draft spar have an identical displacement of 12,000 metric tons and an identical draft of 30 m, as illustrated in Fig. 4. In the following, we use “A” to denote the short-draft spar and “B” to represent our mini-platform. The dimensions of these two platforms are summarized in Table 3.

4.1 Comparison of the RAO's

We compute the RAO's for both platforms, as shown in Fig. 5. It shows that the resonance frequency for spar A falls into the range near 14s which is close to the peak wave period T_p in the Gulf of Mexico (GoM), but our new design has a natural period greater than 20s. The large increase of the natural period is due to the combined effects of reducing waterplane area and increasing added mass by the damping plate. In addition, the response of our design B at the resonance frequency with viscous effect included is reduced significantly compared to that without viscous effect.

Table 3 Dimensions of the short-draft spar A and newly designed mini-platform B

| | $R_1(\text{m})$ | $R_2(\text{m})$ | $R_0(\text{m})$ | $R_3(\text{m})$ | $H_1(\text{m})$ | $H_2(\text{m})$ | $H_3(\text{m})$ | $t(\text{m})$ | $\Delta(\text{t})$ |
|---|-----------------|-----------------|-----------------|-----------------|-----------------|-----------------|-----------------|---------------|--------------------|
| A | 11.3 | 11.3 | N/A | 11.3 | N/A | N/A | N/A | N/A | 12,034 |
| B | 8 | 12.1 | 5 | 17.1 | 2 | 7 | 21 | 0.5 | 12,773 |

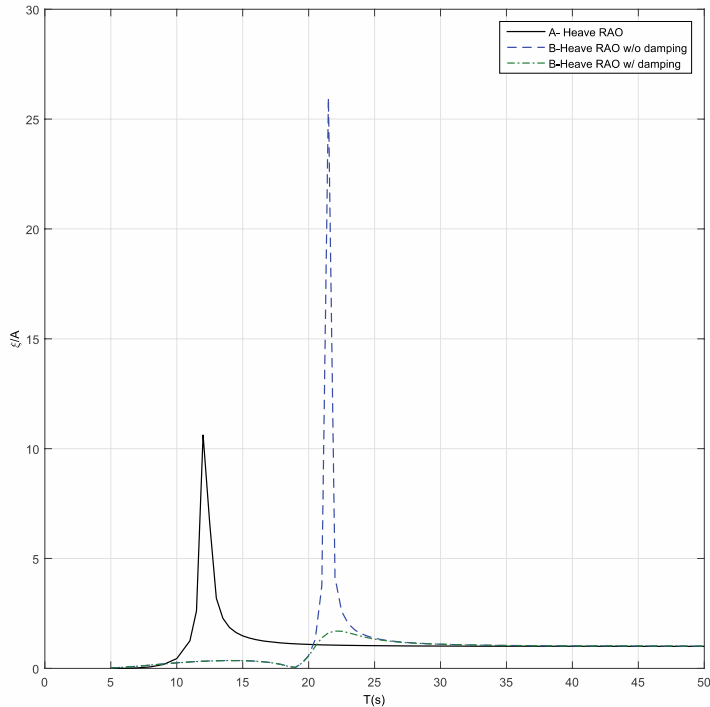


Fig. 5 Comparison of the heave RAO of mini-platform B and spar A (with the incident wave amplitude $\bar{A} = 1$ m). The solid line is the RAO without viscous damping for A while the dashed line is for B. Both of these two lines are obtained from WAMIT. The dash-dot line is the modified RAO with viscous damping defined in Eq. (7) based on the combination of WAMIT and DVRM. The dashed-dot line has a much smaller peak value compared with the other two curves

4.2 Comparison of the response in various sea-states

We here consider two different sea-states for the platform design. One is the operation condition for 1-year waves, while the other is the survival condition for 100-year waves. For Gulf of Mexico, the significant wave height H_s and the peak wave period T_p characterizing these two design conditions are given in Table 4.

The heave motion responses of the spar A and the mini-platform B under these two sea-states are provided in Table 5. We can see that the newly designed mini-platform not only satisfies the basic hydrostatic requirement, but also has a satisfactory motion performance compared to the spar. The natural period of its heave motion is 21.5s, which is far away from the peak periods of the wave spectra under both operation and survival conditions. The significant motion height ξ_s in both two design conditions are greatly suppressed in comparison with those of the spar with the same displacement (and draft).

Table 4 The characteristic parameters of the design condition of the sea-states. H_s is the significant wave height. T_p is the peak period of the wave spectrum. The data is retrieved from International Towing Tank Committee (ITTC)

| Operation Condition | | Survival Condition |
|---------------------|------|--------------------|
| $H_s(m)$ | 4.0 | 12.0 |
| $T_p(s)$ | 10.0 | 14.0 |

Table 5 Comparison of the significant heave motion height ξ_s in various sea-states for short-draft spar A and mini-platform B, where GM denotes the hydrostatic metacentric height, and T_n is the natural period in heave. The result is obtained from the combination of WAMIT and DVRM

| # | $GM(m)$ | $T_n(s)$ | 1-year | 100-year |
|-----------------|---------|----------|------------|------------|
| | | | $\xi_s(m)$ | $\xi_s(m)$ |
| A | 1.84 | 12 | 4.63 | 11.5 |
| B (w/o Damping) | 1.06 | 21.5 | 0.41 | 2.51 |
| B (w/ Damping) | 1.06 | 21.5 | 0.41 | 1.03 |

5. Optimal design for the mini-platforms

The feasible design we obtain above can be further improved via multi-objective optimization. We consider three configurations in this section, as shown in Fig. 6. The first one is the simple shape we developed previously with two cylinders connected by a truncated cone. The second one is a further simplification of the first configuration by removing the bottom cylindrical part. The third one is more complicated, composed of several conical segments. The first two geometries with cylindrical sections may be more desirable in practical construction, but we here also investigate other potential geometries to provide useful options that might prove beneficial in future/different contexts.

5.1 Formulation of the optimization problem

Since we are targeting a miniature platform, we fix the volume of displacement at $V=13,000 m^3$. The thickness of the damping plate is fixed to be m . The optimization variables for the three configurations and their limits are defined in Tables 6 and 7. The limits are selected to provide a rather flexible space for designs but also avoid extremely odd shapes.

The following constraints must be examined for each design.

- (1) Constraint for heave natural period: $T_n \geq 18 s$

A heave natural period of about 18 seconds would be considered low for the target operation areas. Minimizing the motion amplitude is consistent with maximizing the natural period. Therefore, 18 seconds could be a compromise between eliminating unwanted designs and unnecessarily shrinking the solution space.

(2) Constraint for metacentric height

Metacentric height should satisfy the following condition to guarantee the hydrostatic stability: $GM \geq 0.8 \text{ m}$

(3) Constraint for cross-section area

The cross section of the platform should be consistent with a moonpool design. The smallest cross section radius for all the configurations should be not less than 7.0 m.

The purpose of optimization is to seek for an economic design of a satisfactory seakeeping characteristic with the displacement fixed at 13,000 metric tons. It is known that a deep draft increases the cost of construction and installation, but reduces the wave exciting force, thereby suppressing the heave response. Therefore, a small draft and a satisfactory heave motion behavior are mutually conflicting. Our objective is to find a compromise solution between these two goals.

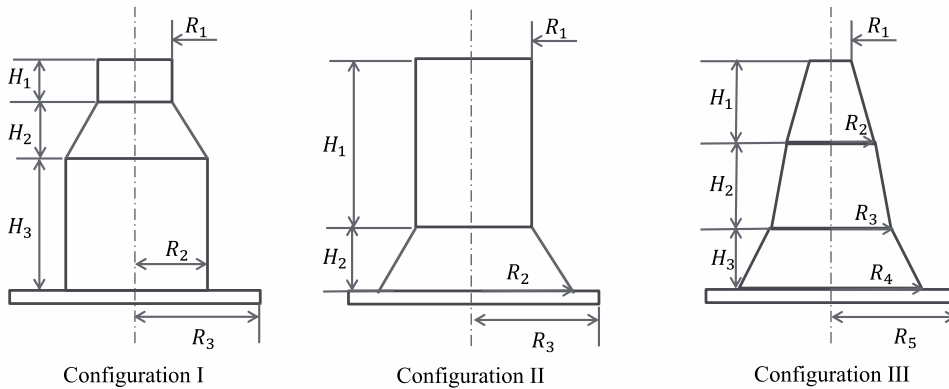


Fig. 6 Sketch of the configurations for the mini-platforms and definition of optimization variables

Table 6 Upper and lower limits of the optimization variables to describe the hull shape for configuration I and II

| No. | Definition | Range |
|-------------------------|-----------------|-------------|
| x_1 | $H/\sqrt[3]{V}$ | 1.06 ~ 1.91 |
| x_2 | H_1/H_2 | 1/5 ~ 5 |
| x_3 (Configuration I) | H_2/H_3 | 1/5 ~ 5 |
| x_4 | R_2/R_1 | 1/3 ~ 3 |
| x_5 | R_3/R_2 | 1.05 ~ 1.5 |

Table 7 Upper and lower limits of the optimization variables to describe the hull shape for configuration III (N=1,2,3)

| No. | Definition | Range |
|------------------|-------------------|-------------|
| x_1 | $H/\sqrt[3]{V}$ | 1.06 ~ 1.91 |
| $x_2(N \geq 2)$ | H_1/H_2 | 1/5 ~ 5 |
| . | . | . |
| . | . | . |
| $x_N (N \geq 2)$ | H_{N-1}/H_N | 1/5 ~ 5 |
| x_{N+1} | R_2/R_1 | 1/2 ~ 2 |
| . | . | . |
| . | . | . |
| x_{2N} | R_{N+1}/R_N | 1/2 ~ 2 |
| x_{2N+1} | R_{N+2}/R_{N+1} | 1.05 ~ 1.5 |

Hence, we choose minimizing both the draft and heave motion amplitude to be our objectives of optimization. Mathematically, the two objective functions $F = [f_1, f_2]$ can be defined as $f_1 = H/\sqrt[3]{V}$ and $f_2 = \xi_s/H_s$ under the survival sea-state condition ($T_p = 14.0$ s, $H_s = 12.0$ m).

5.2 Optimization algorithm

Here we use the so-called ε -multi-objective genetic algorithm (ε -MOGA) (Laumanns *et al.* 2002, Deb 2003) for this multi-objective optimization. This algorithm can provide a finite and small number of optimal results without sacrificing the representativeness, which is suitable for informing decision makers in making the final decision in pragmatic problems. In our problems, the algorithm operates with the real-valued optimization variables with the BLX- α crossover operator and the uniform mutation operator applied. A constraint-domination principle proposed by Deb *et al.* (2001) is used to handle the constraints.

5.3 Results and discussion

5.3.1 Configuration I

For Configuration I, we start with an initial population of 400 designs, and conduct the optimization until the change of the Pareto frontier is negligible, which in this case corresponds to 2400 individuals produced in total. A good variety of initial designs has been created to guarantee that the process will not converge to a single design in the end. The final Pareto frontier for the population of 2400 is shown in Fig. 7.

We can see that there are more than one optimal designs and they are well spread out. The algorithm develops the population and the Pareto frontier toward the ideal solution. Only infeasible solutions exist between the final Pareto frontier and the ideal solution.

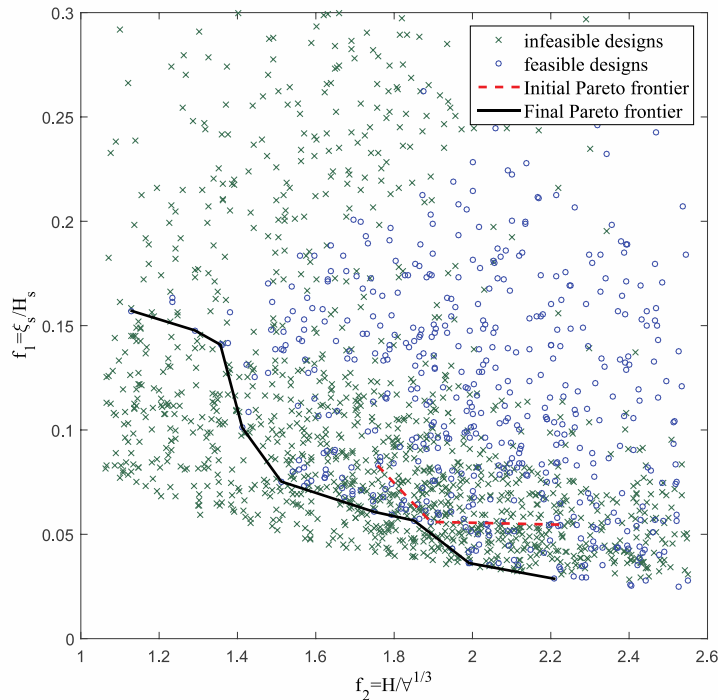


Fig. 7 Pareto frontier evolution for the Configuration I in the objective function space. The black solid line is the final Pareto frontier when the total number of individuals produced reaches 2400, while the red dashed line denotes the initial Pareto frontier

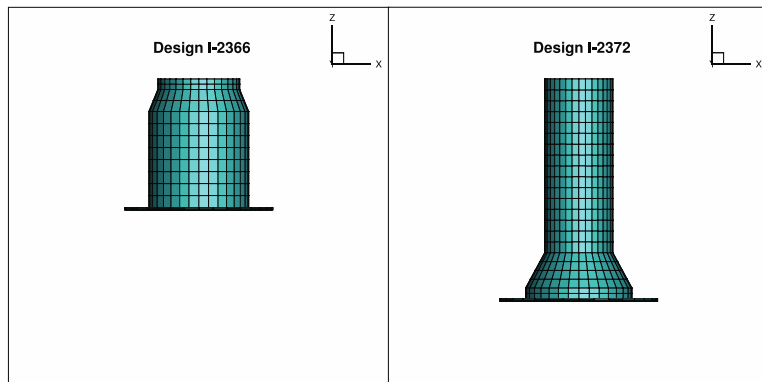


Fig. 8 Selected hull designs of the final Pareto frontier for configuration I. See Table 8 for the detailed dimensions

The final Pareto frontier contains nine designs. Table 8 summarizes the dimensions and properties of these optimal designs. Two representative hull shapes are shown in Fig. 8. Design 2366 features a shallow draft and a relatively high shoulder. However, its seakeeping performance is not satisfactory compared to the other designs in the Pareto frontier.

Table 8 Properties of the optimal designs for Configuration I in the final Pareto frontier after 2400 designs. $T_{n,3}$ and $T_{n,5}$ are the natural periods in heave and pitch, respectively. θ_s^{1yr} and θ_s^{100yr} are the significant pitch motion amplitude under operation condition and survival condition, respectively

| | Design I | | | | | | | | |
|----------------------------|----------|-------|-------|-------|-------|-------|-------|-------|-------|
| | 1921 | 2366 | 2392 | 1936 | 2271 | 1881 | 1480 | 2088 | 2372 |
| $H(m)$ | 26.57 | 30.37 | 31.89 | 33.21 | 35.55 | 41.11 | 43.52 | 46.83 | 51.93 |
| $\xi_s(m)$ | 1.88 | 1.77 | 1.69 | 1.21 | 0.90 | 0.73 | 0.68 | 0.43 | 0.34 |
| $H1(m)$ | 20.29 | 2.45 | 23.51 | 1.12 | 1.15 | 2.88 | 33.9 | 37.10 | 41.07 |
| $H2(m)$ | 5.15 | 5.22 | 6.46 | 5.35 | 5.73 | 13.08 | 7.62 | 7.59 | 8.33 |
| $H3(m)$ | 1.13 | 22.70 | 1.92 | 26.74 | 28.67 | 25.15 | 2.00 | 2.14 | 2.52 |
| $H1/H2$ | 3.94 | 0.47 | 3.64 | 0.21 | 0.20 | 0.22 | 4.45 | 4.89 | 4.93 |
| $H2/H3$ | 4.54 | 0.23 | 3.36 | 0.20 | 0.20 | 0.52 | 3.81 | 3.54 | 3.30 |
| $R1(m)$ | 11.71 | 9.66 | 10.65 | 8.60 | 7.76 | 7.47 | 8.90 | 8.54 | 8.06 |
| $R2(m)$ | 14.52 | 11.79 | 13.32 | 11.27 | 10.94 | 10.53 | 13.09 | 12.98 | 12.57 |
| $R3(m)$ | 21.48 | 17.45 | 19.84 | 16.11 | 16.19 | 15.38 | 18.72 | 18.95 | 18.60 |
| $GM (m)$ | 0.80 | 0.82 | 0.87 | 1.00 | 0.99 | 0.85 | 0.82 | 0.84 | 0.92 |
| $T_{n,3}(s)$ | 18.0 | 18.0 | 18.5 | 19.5 | 21.5 | 21.5 | 21.0 | 22.5 | 23.5 |
| $T_{n,5}(s)$ | 37.0 | 28.0 | 34.0 | 24.0 | 25.0 | 30.0 | 40.0 | 43.0 | 43.0 |
| $\theta_s^{1yr} (\circ)$ | 0.47 | 1.73 | 1.23 | 2.51 | 2.58 | 2.40 | 1.67 | 1.63 | 1.63 |
| $\theta_s^{100yr} (\circ)$ | 0.51 | 2.82 | 1.84 | 4.68 | 5.03 | 4.15 | 2.74 | 2.71 | 2.81 |

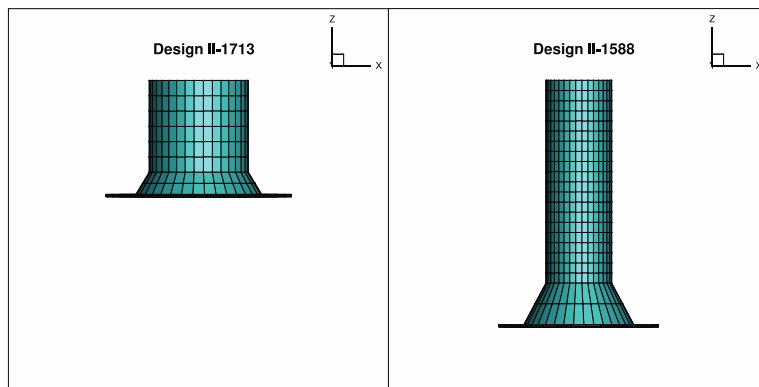


Fig. 9 Selected hull designs of the final Pareto frontier for configuration II. See Table 9 for the detailed dimensions

In addition, the high shoulder may penetrate from the free surface, resulting in instability issues. Design 2372, on the contrary, has the deepest draft and a much lower shoulder.

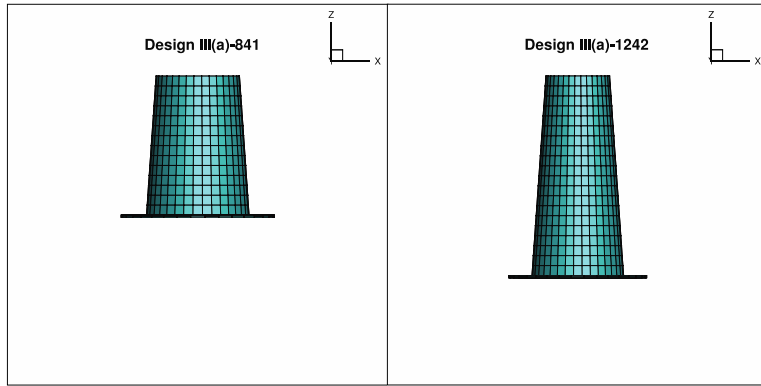


Fig. 10 Selected hull designs of the final Pareto frontier for configuration III(a). See Table 10 for the detailed dimensions

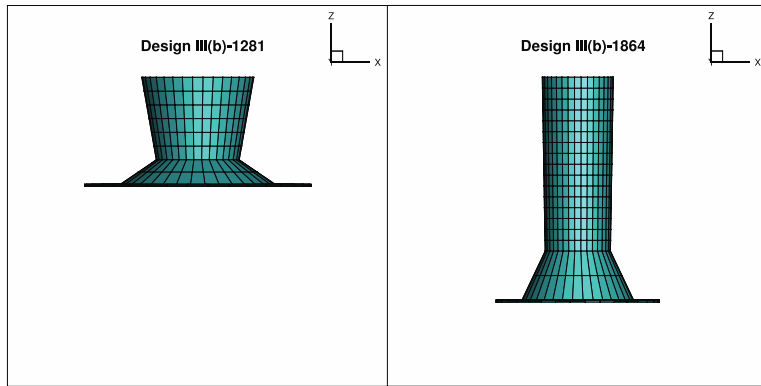


Fig. 11 Selected hull designs of the final Pareto frontier for configuration III(b). See Table 11 for the detailed dimensions

However, it behaves best in heave motion in waves. Its significant heave motion amplitude is about 80.8% smaller than that of design 2366.

5.3.2 Configuration II & III

Similar optimizations are performed for Configuration II and III. For each configuration, two characteristic designs are selected from the final Pareto frontiers (see Figs. 9-12). The dimensions of the optimal designs for each configuration are provided in Tables 10-12. Fig. 13 shows the comparison of the final Pareto frontier for all the configurations.

From the above results we can conclude that:

1. Generally, designs with more degrees of freedom achieve better heave motion behaviors. However, as the draft of the platform increases, the difference in the motion performance for different configurations becomes less significant.
2. From the final Pareto frontier curves we can see that Configuration II not only performs better in both objectives than Configuration I but

also is simpler in construction. The second cylindrical part at the bottom is redundant. In addition, some of the optimal designs in I with a high shoulder may have the instability issue, as mentioned earlier.

3. In the range of shallow draft, the optimum hull shape features a large waterplane area, a wide keel but a thin intermediate part. A large waterplane area can overcome the difficulty in achieving the hydrostatic stability for the shallow-draft floating platforms. However, large waterplane areas are not beneficial for detuning the natural frequencies of the platforms from the peak frequencies of the wave spectrum. Hence such a displacement distribution with a wide keel and a thin body is required to guarantee a large added mass and a cancelling effect in wave exciting force. Therefore, we can see that for platforms with a small draft, III(b) and III(c) behave significantly better than others. Also, we observe that only small improvements are obtained in the final Pareto frontiers from III(b) to III(c). This implies that two segments is adequate for Configuration III. Since it is much easier to construct a cylindrical segment than a conical one, it clearly costs less to construct II compared to III(b), although III(b) performs much better than II in both objectives. A trade-off should be made when determining an optimal design between III(b) and II for platforms with a draft less than 40 m.
4. For designs with a relatively deep draft, the optimal shapes for different configurations are similar: a long thin body with a large keel. Since deep drafts help lower the gravity centre, there is no need to widen the water-plane area for the hydrostatic stability. Distributing as much displacement as possible at the keel to achieve a large added mass is the best choice. Therefore, for platforms with a draft greater than 40 m, the configuration of a long cylinder plus a cone at the keel is already good enough.

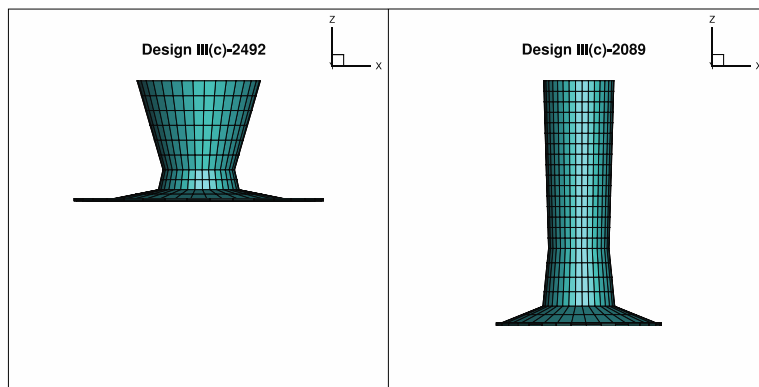


Fig. 12 Selected hull designs of the final Pareto frontier for configuration III(c). See Table 11 for the detailed dimensions

Table 9 Properties of the optimal designs for Configuration II in the final Pareto frontier. $T_{n,3}$ and $T_{n,5}$ are the natural periods in heave and pitch, respectively. θ_s^{1yr} and θ_s^{100yr} are the significant pitch motion amplitude under operation condition and survival condition, respectively

| | Design II | | | | | | | |
|---------------------------|------------------|------------|-------------|-------------|-------------|-------------|-------------|-------------|
| | 1713 | 717 | 1247 | 1692 | 1769 | 1779 | 1994 | 1588 |
| $H(m)$ | 26.92 | 28.03 | 31.6 | 33.38 | 36.67 | 40.32 | 43.98 | 57.66 |
| $\zeta_s(m)$ | 1.58 | 1.35 | 0.96 | 0.85 | 0.74 | 0.53 | 0.47 | 0.31 |
| $H1(m)$ | 21.67 | 22.72 | 25.39 | 27.35 | 28.93 | 32.73 | 35.51 | 47.87 |
| $H2(m)$ | 5.25 | 5.31 | 6.21 | 6.03 | 7.74 | 7.59 | 8.47 | 9.79 |
| $H1/H2$ | 4.13 | 4.28 | 4.09 | 4.54 | 3.74 | 4.31 | 4.19 | 4.89 |
| $R1(m)$ | 11.70 | 11.44 | 10.71 | 10.41 | 9.86 | 9.34 | 8.92 | 7.77 |
| $R2(m)$ | 14.86 | 14.87 | 14.46 | 14.57 | 14.00 | 14.20 | 13.82 | 12.97 |
| $R3(m)$ | 21.85 | 21.87 | 21.55 | 21.27 | 20.58 | 20.73 | 20.18 | 18.80 |
| $GM(m)$ | 0.907 | 0.861 | 0.819 | 0.838 | 0.844 | 0.835 | 0.950 | 1.64 |
| $T_{n,3}(s)$ | 18.5 | 19.0 | 20.0 | 20.5 | 20.5 | 22.0 | 22.5 | 24.5 |
| $T_{n,5}(s)$ | 35.0 | 37.0 | 38.0 | 38.0 | 38.0 | 41.0 | 39.0 | 34.0 |
| $\theta_s^{1yr}(\circ)$ | 0.46 | 0.54 | 0.87 | 1.02 | 1.318 | 1.38 | 1.56 | 1.80 |
| $\theta_s^{100yr}(\circ)$ | 0.50 | 0.61 | 1.17 | 1.42 | 2.00 | 2.14 | 2.55 | 3.35 |

Table 10 Properties of the optimal designs for Configuration III(a) in the final Pareto frontier. $T_{n,3}$ and $T_{n,5}$ are the natural periods in heave and pitch, respectively. θ_s^{1yr} and θ_s^{100yr} are the significant pitch motion amplitude under operation condition and survival condition, respectively

| | Design IIIa | | | | | | |
|---------------------------|--------------------|-------------|------------|-------------|------------|-------------|-------------|
| | 841 | 1281 | 843 | 1008 | 898 | 1124 | 1242 |
| $H(m)$ | 32.82 | 36.78 | 38.42 | 40.33 | 42.69 | 44.57 | 47.12 |
| $\zeta_s(m)$ | 1.76 | 1.31 | 1.02 | 0.85 | 0.70 | 0.58 | 0.52 |
| $R1(m)$ | 9.85 | 9.11 | 8.76 | 8.44 | 8.10 | 7.79 | 7.51 |
| $R2(m)$ | 12.12 | 11.66 | 11.56 | 11.39 | 11.17 | 11.07 | 10.82 |
| $R3(m)$ | 18.06 | 17.37 | 17.22 | 16.97 | 16.76 | 16.49 | 16.24 |
| $GM(m)$ | 0.815 | 0.860 | 0.800 | 0.807 | 0.840 | 0.809 | 0.897 |
| $T_{n,3}(s)$ | 18.0 | 19.0 | 20.0 | 20.5 | 21.0 | 21.5 | 22.5 |
| $T_{n,5}(s)$ | 31.0 | 31.0 | 33.0 | 34.0 | 34.0 | 36.0 | 36.0 |
| $\theta_s^{1yr}(\circ)$ | 1.69 | 1.97 | 1.97 | 2.01 | 2.03 | 2.01 | 2.03 |
| $\theta_s^{100yr}(\circ)$ | 2.71 | 3.28 | 3.27 | 3.37 | 3.47 | 3.44 | 3.54 |

Table 11 Properties of the optimal designs for Configuration III(b) in the final Pareto frontier. $T_{n,3}$ and $T_{n,5}$ are the natural periods in heave and pitch, respectively. θ_s^{1yr} and θ_s^{100yr} are the significant pitch motion amplitude under operation condition and survival condition, respectively

| | Design IIIb | | | | | | |
|---------------------------|--------------------|-------------|-------------|-------------|-------------|-------------|-------------|
| | 1281 | 1839 | 1683 | 1659 | 1629 | 1998 | 1864 |
| $H(m)$ | 25.27 | 28.58 | 29.00 | 39.00 | 41.27 | 46.46 | 52.61 |
| $\zeta_s(m)$ | 0.90 | 0.84 | 0.80 | 0.54 | 0.49 | 0.40 | 0.36 |
| $H_1(m)$ | 19.47 | 21.68 | 22.10 | 30.84 | 33.02 | 35.88 | 41.05 |
| $H_2(m)$ | 5.80 | 6.90 | 6.90 | 8.16 | 8.25 | 10.58 | 11.56 |
| H_1/H_2 | 3.36 | 3.14 | 3.20 | 3.78 | 4.00 | 3.39 | 3.55 |
| $R_1(m)$ | 13.23 | 12.47 | 12.02 | 9.86 | 9.59 | 9.14 | 8.38 |
| $R_2(m)$ | 9.79 | 9.10 | 9.62 | 8.88 | 8.63 | 7.77 | 7.71 |
| $R_3(m)$ | 18.31 | 17.48 | 16.73 | 15.09 | 14.93 | 14.46 | 13.19 |
| $R_4(m)$ | 26.74 | 25.87 | 25.10 | 21.43 | 21.20 | 20.96 | 19.26 |
| $GM(m)$ | 1.243 | 1.069 | 0.904 | 0.826 | 0.924 | 1.000 | 1.419 |
| $T_{n,3}(s)$ | 20.5 | 20.5 | 20.5 | 21.5 | 22.0 | 23.0 | 23.0 |
| $T_{n,5}(s)$ | 40.0 | 43.0 | 44.0 | 42.0 | 41.0 | 42.0 | 35.0 |
| $\theta_s^{1yr}(\circ)$ | 0.38 | 0.26 | 0.30 | 1.22 | 1.34 | 1.46 | 1.77 |
| $\theta_s^{100yr}(\circ)$ | 0.84 | 0.34 | 0.36 | 1.82 | 2.09 | 2.40 | 3.17 |

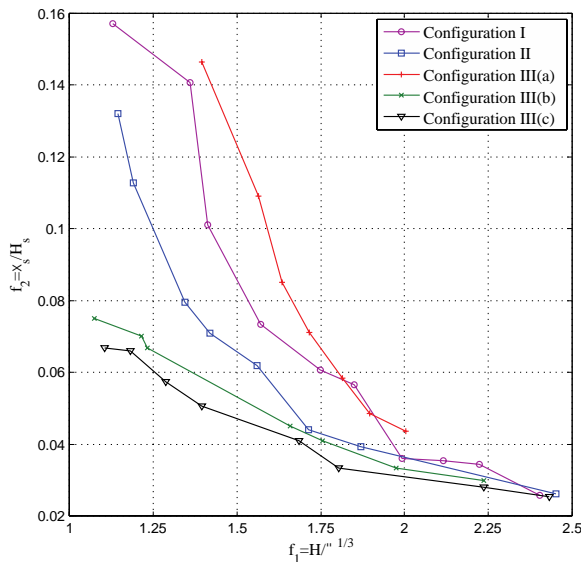


Fig. 13 Comparison of the final Pareto frontier for all the configurations

Table 12 Properties of the optimal designs for Configuration III(c) in the final Pareto frontier. $T_{n,3}$ and $T_{n,5}$ are the natural periods in heave and pitch, respectively. θ_s^{1yr} and θ_s^{100yr} are the significant pitch motion amplitude under operation condition and survival condition, respectively

| | Design IIIc | | | | | | | |
|---------------------------|-------------|-------------|-------------|-------------|-------------|-------------|-------------|-------------|
| | 2328 | 2492 | 1317 | 2106 | 2485 | 1159 | 1638 | 2089 |
| $H(m)$ | 26.00 | 27.79 | 30.29 | 32.83 | 39.61 | 42.40 | 52.58 | 57.19 |
| $\xi_s(m)$ | 0.80 | 0.79 | 0.69 | 0.61 | 0.49 | 0.40 | 0.34 | 0.31 |
| $H_1(m)$ | 19.79 | 20.98 | 22.42 | 12.32 | 29.81 | 4.88 | 34.04 | 39.58 |
| $H_2(m)$ | 5.17 | 4.70 | 6.48 | 15.61 | 7.40 | 24.41 | 14.00 | 13.65 |
| $H_3(m)$ | 1.04 | 2.11 | 1.38 | 4.90 | 2.40 | 13.12 | 4.53 | 3.97 |
| H_1/H_2 | 3.83 | 4.46 | 3.46 | 0.79 | 4.03 | 0.20 | 2.43 | 2.90 |
| H_2/H_3 | 0.58 | 0.58 | 0.55 | 0.51 | 0.56 | 0.68 | 0.82 | 0.86 |
| $R_1(m)$ | 15.30 | 14.56 | 14.47 | 14.85 | 12.56 | 11.39 | 8.88 | 8.30 |
| $R_2(m)$ | 8.88 | 8.44 | 7.96 | 7.57 | 7.03 | 7.74 | 7.28 | 7.14 |
| $R_3(m)$ | 9.50 | 9.54 | 9.15 | 7.73 | 7.95 | 7.05 | 8.60 | 8.50 |
| $R_4(m)$ | 22.13 | 20.14 | 21.51 | 22.02 | 18.28 | 17.13 | 17.62 | 18.36 |
| $R_5(m)$ | 30.54 | 29.40 | 29.03 | 30.16 | 26.51 | 25.35 | 20.61 | 19.46 |
| $GM(m)$ | 4.171 | 3.564 | 4.154 | 3.867 | 4.337 | 2.388 | 1.994 | 2.055 |
| $T_{n,3}(s)$ | 21.0 | 21.0 | 21.0 | 21.5 | 22.0 | 22.5 | 23.5 | 24.0 |
| $T_{n,5}(s)$ | 28.0 | 29.0 | 26.0 | 39.0 | 22.0 | 7.0 | 39.0 | 38.0 |
| $\theta_s^{1yr}(\circ)$ | 0.528 | 0.360 | 0.224 | 0.200 | 1.086 | 0.466 | 1.554 | 1.609 |
| $\theta_s^{100yr}(\circ)$ | 1.141 | 0.821 | 0.380 | 0.424 | 2.972 | 0.563 | 2.74 | 2.938 |

6. Conclusions

The main purpose of this paper is to propose novel and feasible design concepts for small floating platform for deepwater marginal fields development from a hydrodynamic point of view. The design combines the features of a small simple spar-type floater with a heave plate at the keel. The displacement of our design is restricted to around 10,000 metric tons to save cost in construction and installation. We seek platforms that behave better in oscillatory heave motion responses in waves compared to the short-draft (classical) spars at the same displacement.

We utilize the viscous damping effect introduced by the heave plate at the keel to further suppress the heave motion of the mini-platform. A new efficient hydrodynamic model “Discrete Vortex Ring Model” is employed to account for this viscous damping effect. The combination of DVRM and WAMIT serves as a useful design tool to evaluate the dynamic motion performance of our designs. The efficiency and accuracy of this tool enables its integration into an evolutionary algorithm. A multi-objective optimization is then performed to search for the

optimal geometric parameters for the mini platform.

We extend the analysis and optimization to other configurations for the mini platform with the same displacement of 13,000 metric tons. We find that: (1) Two segments are adequate for such a single-body design. Further addition of segments does not help materially. (2) For platforms with draft less than 40m, the optimum hull shape is wide at both waterplane and keel but narrow in the middle part. However, if the cost reduction in construction and installation is considered, a long cylinder with a conical section at the keel is also competitive. (3) For platforms with draft larger than 40 m, the configuration of a long cylinder with a cone at the bottom is adequately satisfactory.

References

- ABS-MODU (2012), Rules for building and classing mobile offshore drilling units.
- Akagi, S.S. and Ito, I. (1984), "Optimal design of semisubmersible form by minimizing its motion in random seas", *J. Mech. Design*, **106**(1), 23-30.
- API-RP2A-WSD, (2000), Recommended practice for planning, designing and constructing fixed offshore platforms: working stress design, in: 21st Edition.
- Bernardinis, B.D., Graham, J. and Parker, K. (1981), "Oscillatory flow around disks and through orifices", *J. Fluid Mech.*, **102**, 279-299.
- Birk, L. (2009), "Application of constrained multi-objective optimization to the design of offshore structure hulls", *J. Offshore Mech. Arct.*, **131**(1), 011301.
- Brown, C. and Michael, W.H., Jr. (1955), On slender delta wings with leading-edge separation.
- Canals, M. and Pawlak, G. (2011), "Three-dimensional vortex dynamics in oscillatory flow separation", *J. Fluid Mech.*, **674**, 408-432.
- Cermelli, C. et al. (2004), "Minifloat: A novel concept of minimal floating platform for marginal field development", *Proceedings of the 14th International Offshore and Polar Engineering Conference*, International Society of Offshore and Polar Engineers.
- Chakrabarti, S. (2005), Handbook of Offshore Engineering (2-volume set).
- Chou, F. (1977), A minimization scheme for the motions and forces of an ocean platform in random seas.
- Clauss, G. and Birk, L. (1996), "Hydrodynamic shape optimization of large offshore structures", *Appl. Ocean Res.*, **18**(4), 157-171.
- Cozijn, H., et al. (2005), Heave, roll and pitch damping of a deepwater calm buoy with a skirt, in: The Fifteenth International Offshore and Polar Engineering Conference, International Society of Offshore and Polar Engineers.
- Deb, K., Mohan, M. and Mishra, S. (2003), "A fast multi-objective evolutionary algorithm for finding well-spread pareto-optimal solutions", KanGAL report 2003002 (2003), 1-18.
- Deb, K., Pratap, A. and Meyarivan, T. (2001), "Constrained test problems for multi-objective evolutionary optimization", Evolutionary Multi-Criterion Optimization, 284-298.
- Faltinsen, O. and Sortland, B. (1987), "Slow drift eddy making damping of a ship", *Appl. Ocean Res.*, **9**(1), 37-46.
- Haslum, H., et al. (1999), "Alternative shape of spar platforms for use in hostile areas", *Proceedings of the Offshore technology conference*, Offshore Technology Conference.
- Hudson, W., et al. (1996), "A small tension leg platform for marginal deepwater fields", *Proceedings of the Offshore Technology Conference*, Offshore Technology Conference.
- Kagemoto, H. (1992), "Minimization of wave forces on an array of floating bodies: the inverse hydrodynamic interaction theory", *Appl. Ocean Res.*, **14**(2), 83-92.
- Kibbee, S., et al. (1999), "Morperth seastar mini-tlp", *Proceedings of the Offshore Technology Conference*, Offshore Technology Conference.

- Kibbee, S., et al. (2002), "New directions in tlp technology", *Proceedings of the Offshore Technology Conference*, Offshore Technology Conference.
- King, B. (1987), Time-domain analysis of wave exciting forces on ships and bodies, Tech. rep., University of Michigan.
- Koon, J., et al. (2002), "Development of the prince field", *Proceedings of the Offshore Technology Conference*, Offshore Technology Conference.
- Lake, M., He, H., Troesch, A., Perlin, M. and Thiagarajan, K. (2000), "Hydrodynamic coefficient estimation for tlp and spar structures", *J. Offshore Mech. Arct.*, **122**(2), 118-124.
- Lamb, H. (1932), Hydrodynamics, Cambridge university press.
- Laumanns, M., Thiele, L., Deb, K. and Zitzler, E. (2002), "Combining convergence and diversity in evolutionary multiobjective optimization", *Evol. Comput.*, **10**(3), 263-282.
- Lee, X. (1995), WAMIT theory manual, Massachusetts Institute of Technology, Department of Ocean Engineering.
- Mei, C., Stiassnie, M. and Yue, D. (2005), Theory and applications of ocean surface waves: Linear aspects.
- Miao, S. (2013), Design of miniature floating platform for marginal fields, Ph.D. thesis, Massachusetts Institute of Technology.
- Michel, W. (1999), "Sea spectra revisited", *Mar. Technol.*, **36**(4), 211-227.
- Newman, J. (1977), Marine hydrodynamics, MIT press.
- Newman, J. (1992), Panel methods in marine hydrodynamics, in: Proc. Conf. Eleventh Australasian Fluid Mechanics-1992.
- Newman, J. and Lee, C. (2002), "Boundary-element methods in offshore structure analysis", *J. Offshore Mech. Arct.*, **124**(2), 81-89.
- Newman, J. and Sclavounos, P. (1988), "The computation of wave loads on large offshore structures", *Proceedings of the Int. Conf. on Behaviour of Offshore Structures (BOSS88)*.
- Nitsche, M. and Krasny, R. (1994), "A numerical study of vortex ring formation at the edge of a circular tube", *J. Fluid Mech.*, **276**, 139-161.
- Ronalds, B., et al. (2002), "Deepwater facility selection", *Proceedings of the Offshore Technology Conference*, Offshore Technology Conference.
- Sadeghi, K., Incecik, A. and Downie, M. (2004), "Response analysis of a truss spar in the frequency domain", *J. Marine Sci. Tech.*, **8**(3) (2004) 126-137.
- Stiassnie, M., Naheer, E. and Boguslavsky, I. (1984), "Energy losses due to vortex shedding from the lower edge of a vertical plate attacked by surface waves", *Proceedings of the Royal Society of London A: Mathematical, Physical and Engineering Sciences*, **396**, 131-142.
- Wilhoit, L. and Supan, C. (2010), Worldwide survey of tlps, tlwps, Offshore Magazine.

MK